



Schiff's bases derived from L-lysine and aromatic aldehydes as green corrosion inhibitors for mild steel: Experimental and theoretical studies



Neeraj Kumar Gupta, Chandrabhan Verma, M.A. Quraishi*, A.K. Mukherjee

Department of Chemistry, Indian Institute of Technology, Banaras Hindu University, Varanasi 221005, India

ARTICLE INFO

Article history:

Received 29 July 2015

Received in revised form 21 November 2015

Accepted 8 December 2015

Available online xxxx

Keywords:

GREEN SCHIFF'S BASES

Mild steel

Acid corrosion

SEM/EDX/AFM

ABSTRACT

Three Schiff's bases (SBs) namely, 2-amino-6-(2-hydroxybenzylideneamino) hexanoic acid (SB-1), 2-amino-6-(4-methoxybenzylideneamino) hexanoic acid (SB-2) and 2-amino-6-((4-dimethylamino)benzylideneamino) hexanoic acid (SB-3) derived from lysine (amino acid) and three different aldehydes were synthesized and evaluated as corrosion inhibitors for mild steel in 1 M HCl solution using weight loss, electrochemical, scanning electron microscopy (SEM), energy dispersive X-ray spectroscopy (EDX) and atomic force microscopy methods. The results showed that inhibition efficiency increases with the increasing concentration. Among the studied SBs the SB-3 showed maximum inhibition efficiency of 95.6% at 400 mg L⁻¹ concentration. Potentiodynamic polarization study revealed that the investigated SBs act as cathodic type inhibitors. Adsorption of the SBs on mild steel surface obeys the Langmuir adsorption isotherms. The weight loss and electrochemical results were well supported by SEM, EDX and AFM analyses.

© 2015 Elsevier B.V. All rights reserved.

1. Introduction

Mild steel is widely used in several industries as construction material due to its high mechanical properties and low cost [1,2]. However, it is a highly reactive alloy and is very prone to corrosion during many industrial processes including acid cleaning, etching, acid pickling, and acid descaling [3,4]. Among the various available methods of corrosion protection, the consumption of the synthetic corrosion inhibitors is one of the most practical and cost effective method [5,6]. Generally, organic inhibitors inhibit metallic corrosion by adsorbing on the surface and thereby forming a protective barrier between metal and electrolyte (1 M HCl) [7]. The adsorption of these inhibitors on metallic surface are influenced by several factors such as molecular size of inhibitor, nature of substituents, nature of metal and electrolyte [8–10]. Organic compounds containing heteroatoms including nitrogen, sulfur, and/or oxygen with polar functional groups and conjugated double bonds have been reported as effective corrosion inhibitor [11]. The Schiff's bases are important class of compounds characterized by the presence of –CH=N– group. Schiff's bases constitute potential class of corrosion inhibitors and besides this they have many interesting properties and extensive applications in medicinal, agricultural, pharmaceutical fields and material science. Due to the great flexibility and diverse structural aspects, a wide range of Schiff bases have been synthesized and utilized as corrosion inhibitors for metal in aggressive media [12–21]. Most of the available Schiff's base inhibitors are toxic in nature and should be

replaced by environmental friendly non-toxic inhibitors. Amino acid based Schiff's bases are safe and environmentally benign corrosion inhibitors [22–25]. Previously, some Schiff base compounds have been studied which have shown good inhibition efficiency (70–98%) in the concentration range of 350–2700 ppm [26–28]. In view of above observation it is thought worthwhile to synthesize three Schiff's bases from lysine (amino acid) with three different aldehydes namely, 2-amino-6-(2-hydroxybenzylideneamino) hexanoic acid (SB-1), 2-amino-6-(4-methoxybenzylideneamino) hexanoic acid (SB-2), 2-amino-6-(4-methylamino) benzylideneamino) hexanoic acid (SB-3) to investigate their corrosion inhibition properties on mild steel in 1 M HCl solution. In our case, the best inhibition efficiency (95.6%) was shown by SB-3 at 400 ppm. The choice of these compounds is based on the facts that: (a) they can be synthesized from commercially available cheap and green starting materials, (b) they are likely to show good inhibition efficiency, (c) they have aromatic ring, –CH=N– and hetero-atoms (N, O) through which they can adsorb on the metal surface and inhibit corrosion, and (d) the presence of the –CH=N– group in Schiff bases increases their adsorption ability.

2. Experimental section

2.1. Synthesis of corrosion inhibitor

The SBs used in present study were synthesized according to a method described earlier [29]. The synthetic scheme for SBs is shown in Fig. 1. The purity of the synthesized SBs was determined by thin-layer chromatography using ethyl acetate/n-hexane (4:6) on the silica plate TLC

* Corresponding author.

E-mail addresses: maquraishi.apc@itbhu.ac.in, maquraishi@rediffmail.com (M.A. Quraishi).

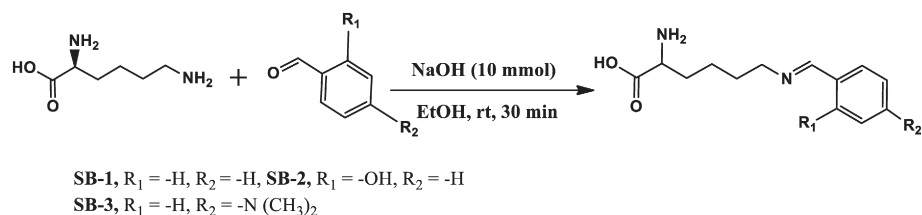


Fig. 1. Synthetic route for investigated SBs.

Table 1
IUPAC name, molecular structure, molecular formula, melting point and analytical data of studied SBs.

S. No.	Name of inhibitor	Chemical structure	Analytical data
1	2-Amino-6-(2-hydroxybenzylideneamino) hexanoic acid (SB-1)		$C_{13}H_{18}N_2O_3$ (mol. wt. 250.29); IR (KBr cm^{-1}): 3663, 3534, 2848, 2288, 1776, 1733, 1680, 1678, 926, 787, 645; 1H NMR (300 MHz, DMSO) δ (ppm): 1.58, 1.67, 1.74, 3.42, 3.71, 6.87, 7.27, 7.42, 8.88, 9.42
2	2-Amino-6-(4-methoxybenzylideneamino) hexanoic acid (SB-2)		$C_{14}H_{20}N_2O_3$ (mol. wt. 264.14); IR (KBr cm^{-1}): 3665, 3491, 2854, 2358, 1783, 1635, 1250, 1163, 960, 823, 621; 1H NMR (300 MHz, DMSO) δ (ppm): 1.25, 1.57, 1.85, 3.58, 3.71, 5.15, 7.41, 7.52, 7.73, 8.57
3	2-Amino-6-((4-dimethylamino)benzylideneamino) hexanoic acid (SB-3)		$C_{15}H_{23}N_3O_2$ (mol. wt. 277.36); IR (KBr cm^{-1}): 3649, 3565, 2818, 2334, 1794, 1741, 1707, 1690, 945, 790, 626; 1H NMR (300 MHz, DMSO) δ (ppm): 1.27, 1.78, 1.93, 3.09, 3.79, 4.54, 5.14, 6.32, 7.54, 8.98

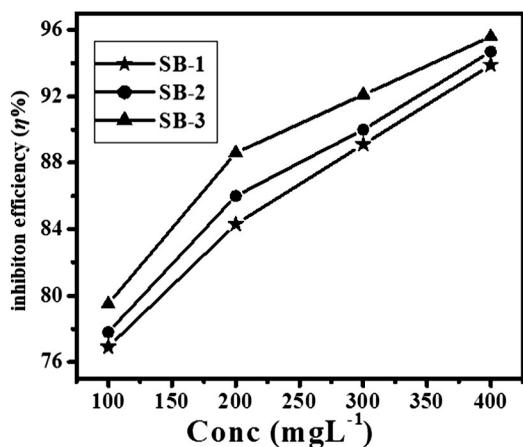


Fig. 2. Variation of inhibition efficiency with SBs concentration.

Table 2
The weight loss parameters derived for mild steel in 1 M HCl at different concentrations of SBs.

Inhibitor	Conc (mg L ⁻¹)	C_R (mg cm ⁻² h ⁻¹)	Surface coverage (θ)	$\eta\%$
Blank	0.0	7.66	–	–
SB-1	100	1.76	0.770	77.0
	200	1.20	0.844	84.4
	300	0.83	0.891	89.1
	400	0.46	0.939	93.9
SB-2	100	1.70	0.778	77.8
	200	1.06	0.861	86.1
	300	0.73	0.904	90.4
	400	0.40	0.947	94.7
SB-3	100	1.56	0.796	79.6
	200	0.86	0.887	88.7
	300	0.60	0.921	92.1
	400	0.33	0.956	95.6

Table 3
Variation of corrosion rate with temperature in absence and presence of optimum concentration of SBs.

Temperature (K)	Corrosion rate (C_R) (mg cm ⁻² h ⁻¹)			
	Blank	SB-1	SB-2	SB-3
308	7.60	0.46	0.40	0.33
318	11.0	2.03	1.90	1.73
328	14.3	3.40	3.13	2.96
338	18.6	5.73	5.43	5.23

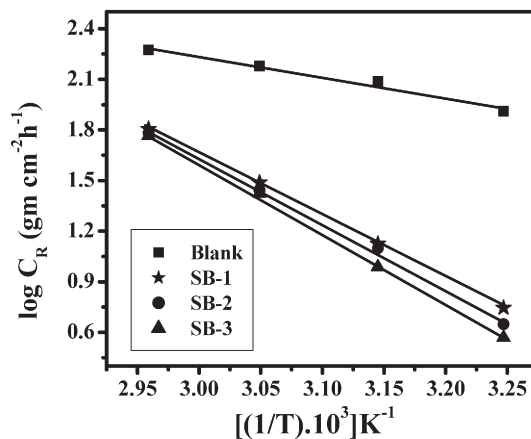
Fig. 3. Arrhenius plots of $\log C_R$ versus $1000/T$ for mild steel corrosion in 1 M HCl solution in absence and presence of SBs.

Table 4
Activation parameters for mild steel dissolution in 1 M HCl in the absence and presence of optimum concentration of SBs.

Inhibitor	E_a (kJ mol ⁻¹)
Blank	28.48
SB-1	70.67
SB-2	74.71
SB-3	80.26

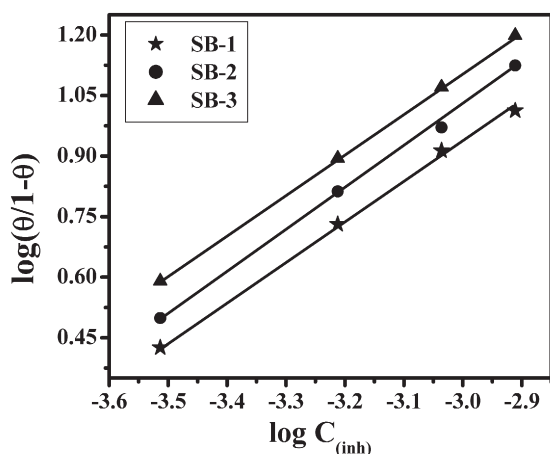


Fig. 4. Langmuir adsorption plot for mild steel in 1 M HCl solution in presence SBs.

Table 5

The values of K_{ads} and ΔG_{ads}° for mild steel in absence and presence of optimum concentration of SBs in 1 M HCl at different temperature.

Inhibitor	K_{ads} ($10^3 M^{-1}$)				$-\Delta G_{ads}^{\circ}$ (kJ mol $^{-1}$)			
	308	318	328	338	308	318	328	338
SB-1	18.4	5.20	3.57	2.33	35.45	33.29	33.27	33.09
SB-2	21.4	5.73	3.97	2.52	35.82	33.81	33.56	33.31
SB-3	26.0	6.39	4.25	2.67	36.33	33.89	33.75	33.47

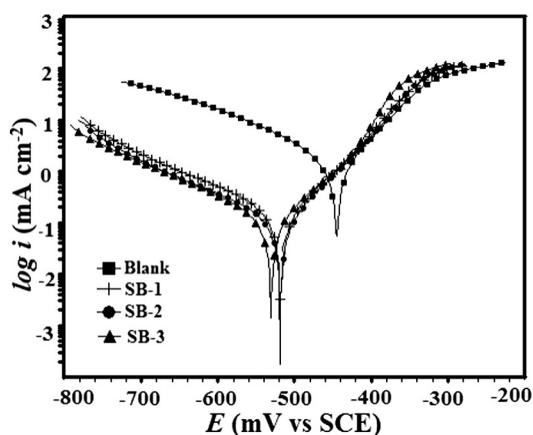


Fig. 5. Potentiodynamic polarization plots for mild steel in 1 M HCl solution in the absence and presence of optimum concentration of SBs.

plates aluminum (Al) silica. The chemical structure, IUPAC name and analytical data of synthesized SBs are given in Table 1.

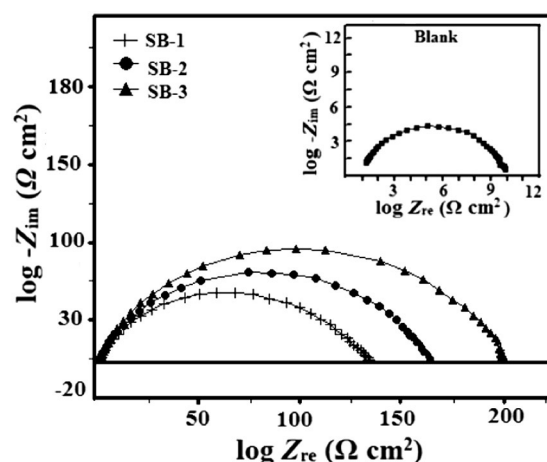
2.2. Materials and chemicals

The mild steel specimens with chemical composition (wt.%): C = 0.076, Mn = 0.192, P = 0.012, Si = 0.026, Cr = 0.050, Al = 0.023 and

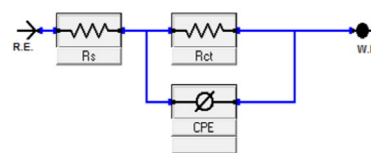
Table 6

Tafel Polarization parameters for mild steel in 1 M HCl solution in absence and presence of optimum concentration of SBs.

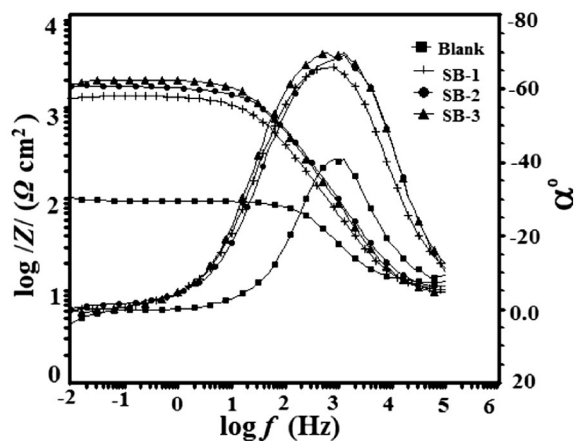
Inhibitor	E_{corr} (mV/SCE)	i_{corr} ($\mu A cm^{-2}$)	β_a (mV/dec)	β_c (mV/dec)	θ	$\eta(\%)$
Blank	-445	1150	70.5	114.6	-	-
SB-1	-519	98.5	83.3	143.9	0.9143	91.43
SB-2	-531	91.8	90.7	151.5	0.9201	92.01
SB-3	-519	64.2	70.20	121.9	0.9441	94.41



(a)



(b)



(c)

Fig. 6. (a–c): (a) Nyquist plots for mild steel in 1 M HCl solution in the absence and presence of an optimum concentration of SBs. (b) Equivalent circuit used to fit the EIS data for mild steel in 1 M HCl solution. (c) Bode plots for mild steel in 1 M HCl solution in the absence and presence of SBs at optimum concentration.

balance Fewere used for chemical, electrochemical and surface experiments. The specimens' size was 2.5 × 2 × 0.025 cm and 8 × 1 × 0.025 cm for weight loss and electrochemical experiments, respectively. The aggressive test solution of 1 M HCl solution was

Table 7

Electrochemical impedance parameters obtained from EIS measurements for mild steel in 1 M HCl in absence and presence of optimum concentration of SBs.

Inhibitor	R_s (Ωcm^2)	R_{ct} (Ωcm^2)	C_{dl} ($\mu F cm^{-2}$)	n	θ	$\eta\%$
Blank	1.12	9.58	106.21	0.827	-	-
SB-1	0.96	129.04	37.92	0.829	0.9257	92.57
SB-2	0.99	164.90	27.75	0.840	0.9419	94.19
SB-3	0.88	197.91	26.63	0.852	0.9515	95.15

prepared by dilution of analytical grade HCl (37%) with double distilled water.

2.3. Gravimetric experiment

The weight loss experiments were performed using the standard method described earlier [27]. The corrosion rate was calculated using equation:

$$C_R = \frac{W}{At} \quad (1)$$

where W is the mean value of weight loss of three parallel mild steel coupons, A is the total area of a mild steel coupon, and t is the immersion time (3 h). The percentage of inhibition efficiency ($\eta\%$) and surface coverage (θ) was calculated from the evaluated corrosion rates using following relation:

$$\eta\% = \frac{C_R - C_{R(i)}}{C_R} \times 100 \quad (2)$$

$$\theta = \frac{C_R - C_{R(i)}}{C_R} \quad (3)$$

where C_R and $C_{R(i)}$ are the corrosion rate ($\text{mg cm}^{-2} \text{h}^{-1}$) values of mild steel coupons in the absence and presence of inhibitors, respectively.

2.4. Electrochemical experiment

Electrochemical measurements were performed by the method as described previously [30]. The electrochemical impedance measurements (EIS) were performed on mild steel specimens in the frequency range of 100 kHz to 0.01 Hz under potentiostatic conditions using an AC at open circuit potential with amplitude of 10 mV peak to peak. The charge transfer resistance was calculated from Nyquist plot from which corrosion inhibition efficiency was calculated using following equation:

$$\eta\% = \frac{R_{ct}^i - R_{ct}^0}{R_{ct}^i} \times 100 \quad (4)$$

where R_{ct}^i and R_{ct}^0 are charge transfer resistances in presence and absence of SBs, respectively.

The potentiodynamic polarization studied were performed on mild steel specimens by automatically changing the electrode potential from -250 to $+250$ mV/SCE versus open circuit potential at a scan rate of 1 mV s^{-1} . The corrosion current density (i_{corr}) was calculated by extrapolating the linear segments of the cathodic and anodic Tafel slopes from which corrosion inhibition efficiency was calculated using following equation:

$$\eta\% = \frac{i_{corr}^0 - i_{corr}^i}{i_{corr}^0} \times 100 \quad (5)$$

where, i_{corr}^0 and i_{corr}^i are the corrosion current densities in absence and presence of SBs.

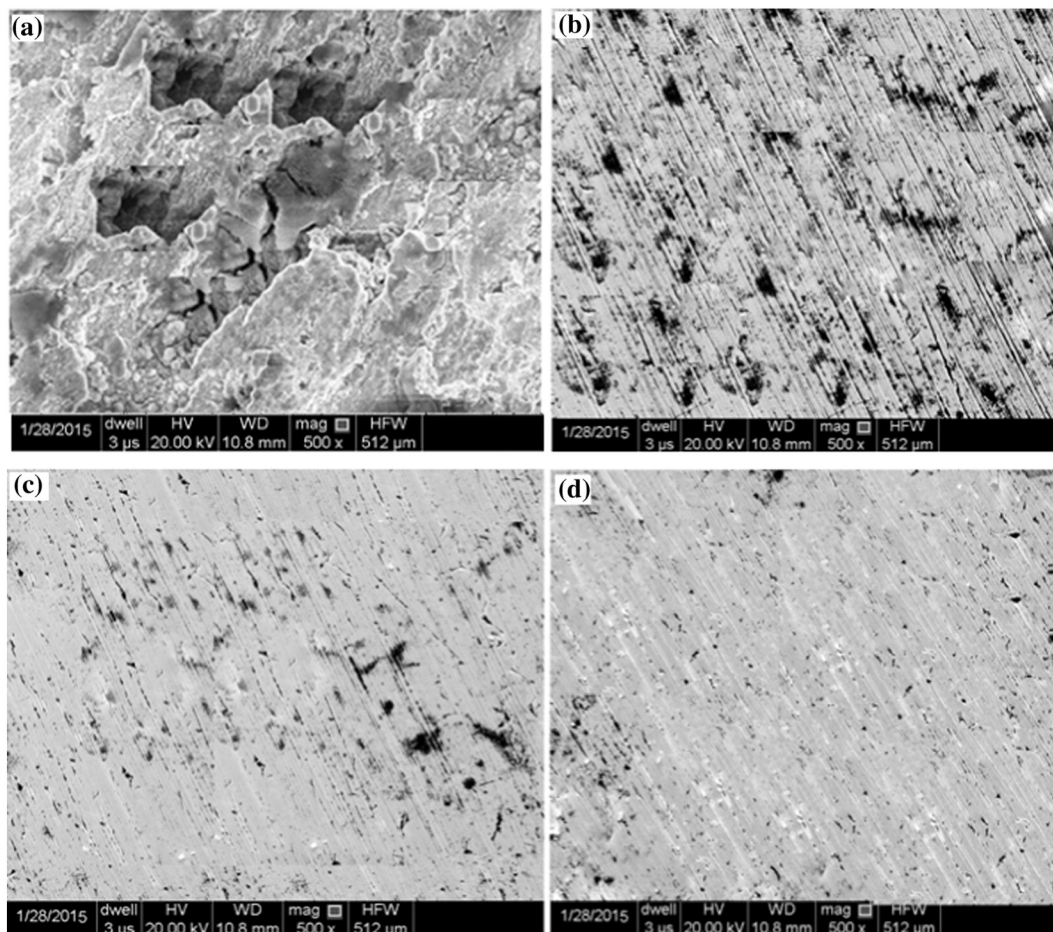


Fig. 7. (a–d): SEM image of mild steel surface after 3 h immersion (a) without SBs, (b) with SB1, (c) with SB2, (d) with SB3.

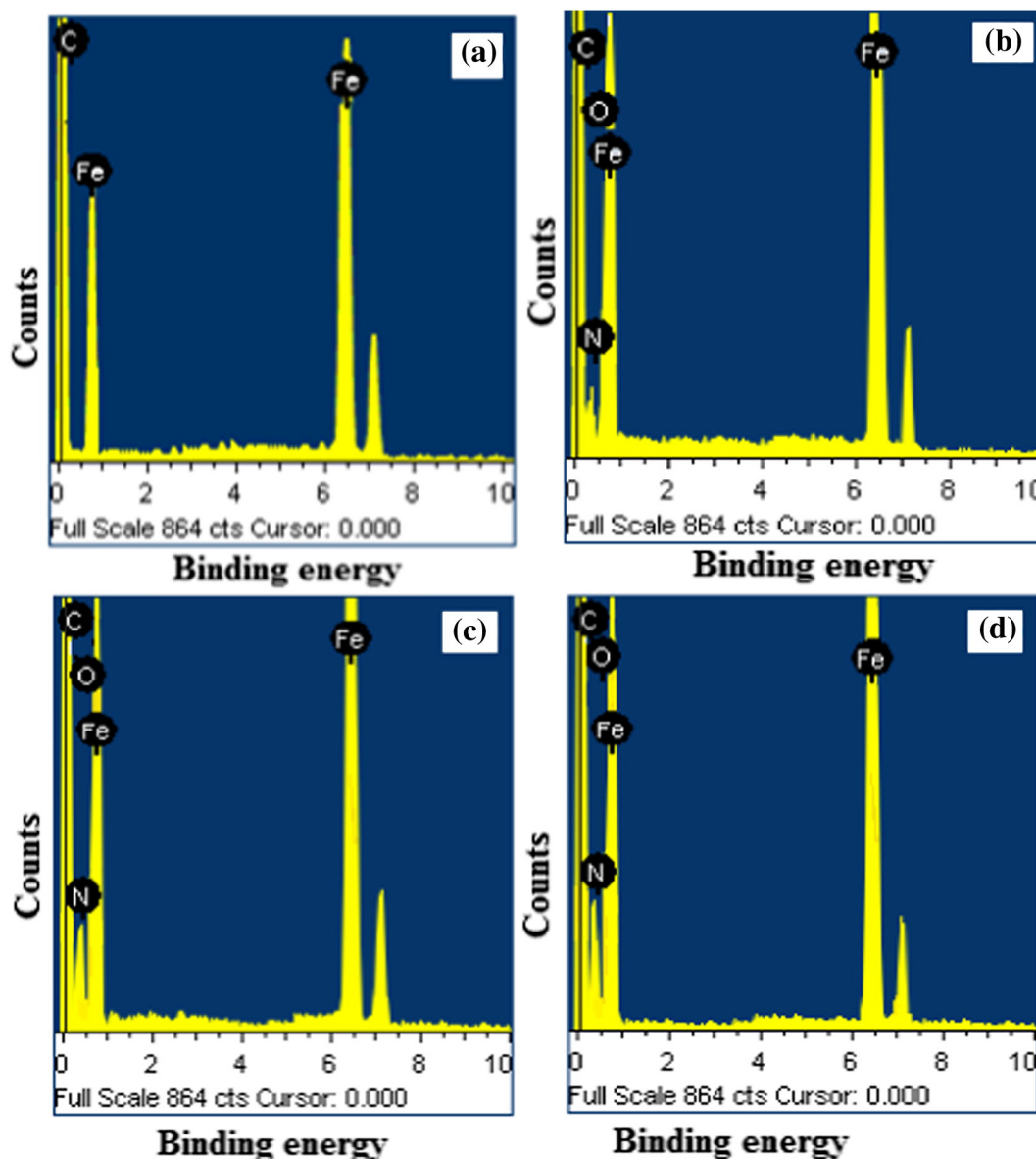


Fig. 8. (a–d): EDX image of mild steel surface after 3 h immersion (a) without SBs, (b) with SB1, (c) with SB2, (d) with SB3.

2.5. SEM/EDX study

The mild steel was immersed in 1 M HCl solution in absence and presence of optimum concentration of the SBs for 3 h immersion time. Thereafter, the mild steel specimens were taken out, washed with double distilled water, dried and finally analyzed by SEM and EDX method. The SEM study was carried out using a Zeiss Evo 50 XVP instrument at an accelerating voltage of 5 kV and 500× magnification.

Table 8

Percentage atomic contents of elements obtained from EDX spectra for SBs.

Inhibitor	Fe	C	N	O
Blank	63.09	36.10	–	–
SB-1	62.43	29.31	8.37	–
SB-2	61.73	23.84	7.89	6.48
SB-3	59.54	22.65	8.36	9.54

2.6. AFM analysis

The AFM analysis was performed using NT-MDT multimode AFM, Russia, controlled by Solver scanning probe microscope controller. The single beam cantilever having resonance frequency in the range of 240–255 kHz in semi-contact mode with corresponding spring constant of 11.5 Nm^{-1} containing NOVA program was used for image interpretation. The scanning area in the images was $10 \mu\text{m} \times 10 \mu\text{m}$.

3. Result and discussion

3.1. Weight loss experiment

3.1.1. Effect of SBs concentration

The variation of $\eta\%$ with SBs concentration is shown in Fig. 2 and several weight loss parameters are given in Table 2. From the results it is clear that inhibition efficiency increases on increasing SBs concentration and maximum efficiency was obtained at 400 mg L^{-1} concentration. The order of inhibition efficiency of studied SBs follows the order: SB-

3 > SB-2 > SB-1. The increase in $\eta\%$ on increasing SBs concentration is due to increase in the surface coverage.

3.1.2. Effect of temperature

To evaluate the effect of temperature on the inhibition efficiency, the weight loss experiments were also performed in the temperature range of 308–338 K. The variation of corrosion rate (C_R) with temperature is represented in Table 3. From the results it can be observed that $\eta\%$ decreases with increasing temperature. The increase in temperature resulted into desorption of the adsorbed SBs molecules from the mild steel surface resulting into decrease in $\eta\%$ [31]. The effect of temperature on corrosion rate can be best represented by Arrhenius equation [32]:

$$C_R = A \exp\left(\frac{-E_a}{RT}\right) \quad (6)$$

where, E_a is the apparent activation energy, T is the absolute temperature, A is the Arrhenius pre-exponential constant and R is the gas constant. The Arrhenius plots of $\log C_R$ vs $1/T$ of mild steel 1 M HCl solution is shown in Fig. 3 from which the values of E_a were calculated from the slope and listed in Table 4. The tabulated data revealed that value of E_a for inhibited solution is greater than that of uninhibited solution. This increase in E_a in presence of SBs indicates the formation of higher energy barrier for corrosion process suggesting that adsorbed film of SBs film on mild steel surface prevents the charge/mass transfer

reaction occurring on the surface [33,34]. Moreover, the decrease in inhibition efficiency with increasing temperature signify the physical adsorption that occurs during first stage of adsorption process [34]. The increased value of E_a also suggest that presence of SBs rate of mild steel dissolution decreased due to formation of metal-inhibitor complex [34].

3.1.3. Adsorption isotherms and thermodynamic consideration

The adsorption isotherm is very important in understanding the mechanism of interaction between metal surface and the inhibitor [35]. Several adsorption isotherms were tested among which Langmuir isotherm gave the best fit with values of regression coefficient (R^2) very close to unity. The values of regression coefficient were 0.9998, 0.9998 and 0.9999 for SB-1, SB-2 and SB-3, respectively. The Langmuir isotherm can be represented as follows [36]:

$$\frac{C_{(inh)}}{\theta} = \frac{1}{K_{(ads)}} + C_{(inh)} \quad (7)$$

where, K_{ads} is the constant for adsorption–desorption processes occurring on metal surface, θ is the surface coverage and $C_{(inh)}$ is the SBs concentration in mg L^{-1} . The Langmuir isotherm plot (Fig. 4) gives a straight line between $\log(\theta/1-\theta)$ and $C_{(inh)}$ and the value of K_{ads} was calculated and given in Table 4. The K_{ads} values related with the free energy

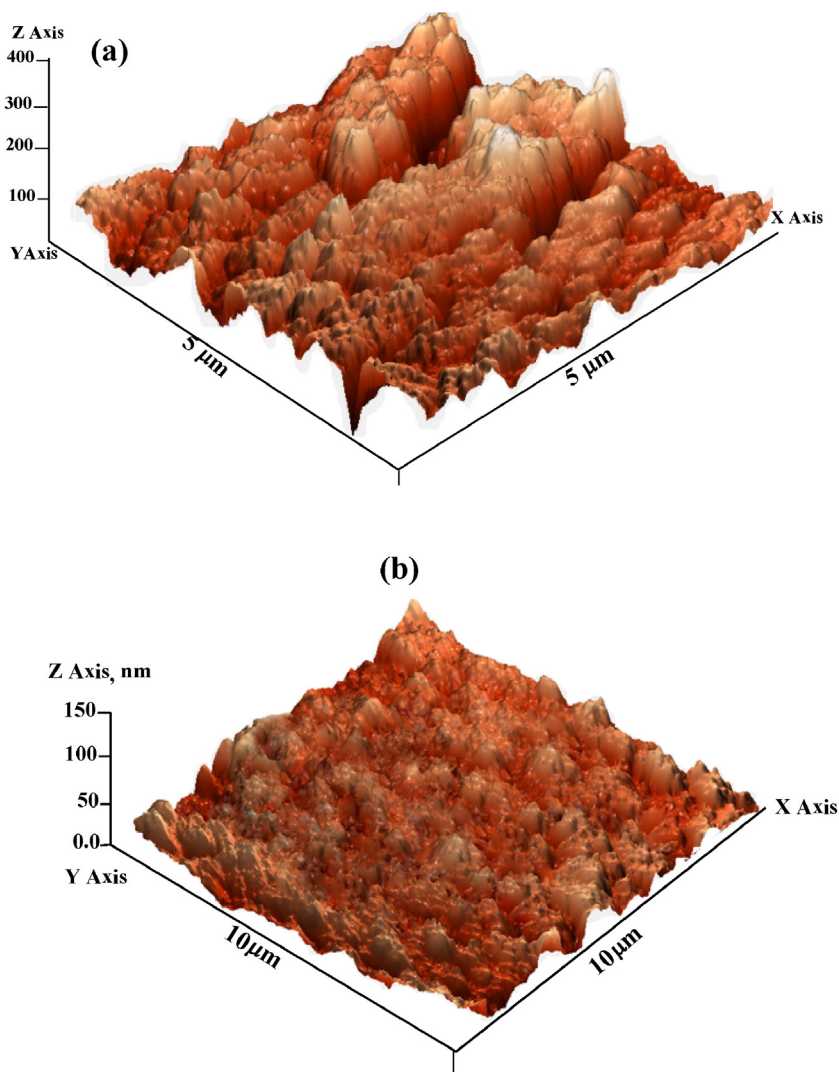


Fig. 9. (a–d): 3D AFM image of mild steel surface after 3 h immersion (a) without SBs, (b) with SB1, (c) with SB2, (d) with SB3.

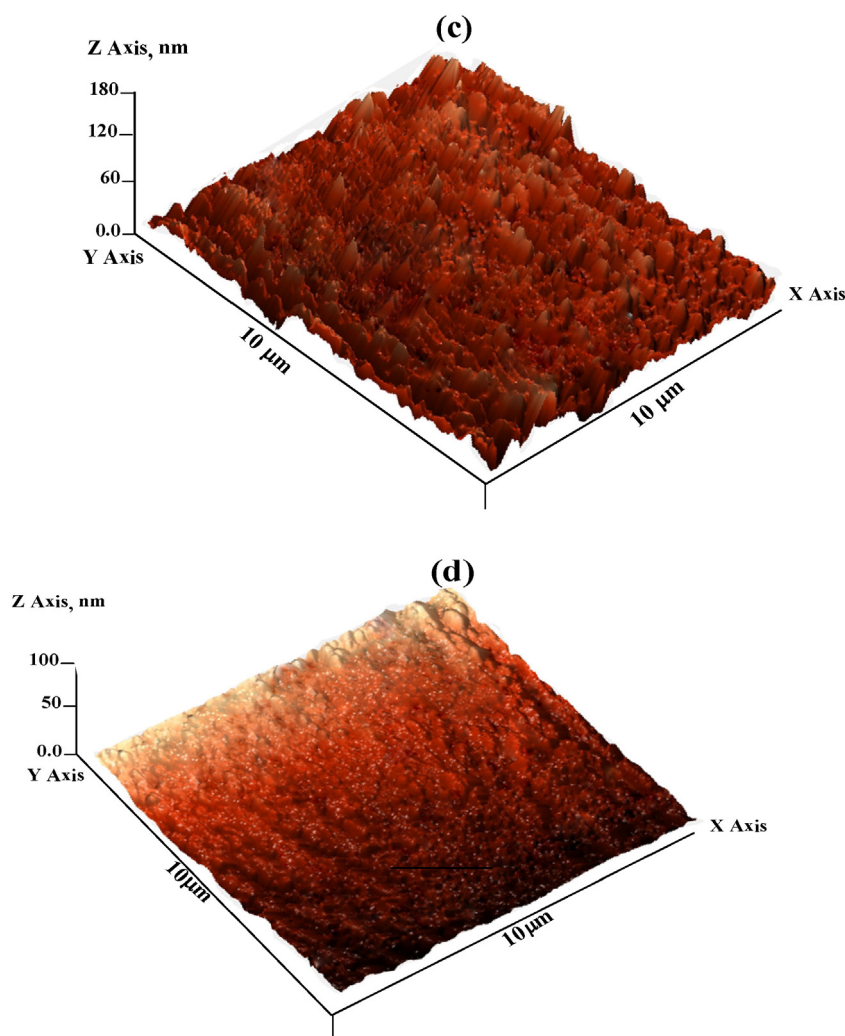


Fig. 9 (continued).

of adsorption (ΔG_{ads}^0) according to the relation [36]:

$$\Delta G_{\text{ads}}^0 = -RT \ln(55.5K_{\text{ads}}) \quad (8)$$

where, R is the universal gas constant, T is the absolute temperature and value 55.5 represent the molar concentration of water in acid solution. The calculated values of ΔG_{ads}^0 are given in Table 5. The value of ΔG_{ads}^0 for SBs lies in the range -33.09 to -36.33 kJ mol^{-1} . These values are in between the threshold values for physical and chemical adsorption suggesting that the adsorption of SBs on mild steel surface involves both chemical and physical adsorption [31,37].

3.2. Electrochemical measurements

3.2.1. Polarization study

The Tafel polarization curves obtained for mild steel in absence and presence of SBs at optimum concentration are shown in Fig. 5. Table 6 represents the polarization parameters i.e., corrosion potential (E_{corr}), cathodic (β_c) and anodic (β_a) Tafel slopes, corrosion current density (i_{corr}), surface coverage (θ) and the inhibition efficiency ($\eta\%$) for mild steel corrosion with and without SBs. The results showed that in presence of SBs corrosion current density is decreased due to formation of protective film [38]. It is also observed that the addition of SBs retards both cathodic and anodic reactions; however, the cathodic reactions are comparatively more affected than the anodic reactions suggesting

that investigated SBs are mixed type inhibitors and predominantly act as cathodic inhibitors [39].

3.2.2. Electrochemical impedance spectroscopic study

Fig. 6(a) represents the Nyquist plots for mild steel in 1 M HCl solution in absence and presence of optimum concentration of the SBs. From the Fig. 6(a) it could be observed that Nyquist plots give similar appearance with and without SBs suggesting that SBs inhibit mild steel corrosion without affecting the mechanism [40]. The Nyquist plot consists of a depressed semicircle at high frequency region which is a characteristic response of solid metal electrodes in the corrosion process [41]. Impedance parameters such as R_{ct} , n , C_{dl} , θ and $\eta\%$ were derived from Nyquist plot by implying equivalent circuit shown in Fig. 6(b) and given in Table 7. The result showed that addition of SBs causes significant increase in the R_{ct} value suggesting that SBs retard the charge transfer reaction and corrosion occurring on the mild steel surface by forming protective film on the surface [42]. From the results it is also clear that values of C_{dl} decreased in presence of SBs. The decrease in C_{dl} value is due to the decrease in local dielectric constant and/or an increase in the thickness of the electrical double layer. This increase in thickness of electric double layer is due to the adsorption of the SBs on the surface. This finding further suggests that the inhibition of mild steel corrosion is due to adsorption mechanism [43]. The value of n is related to surface roughness. Generally surface roughness increases with the decrease in the value of n [44]. It can be observed that the values on n in presence of SBs are larger (0.829 for SB-1, 0.840 for SB-2 and 0.852 for SB-3)

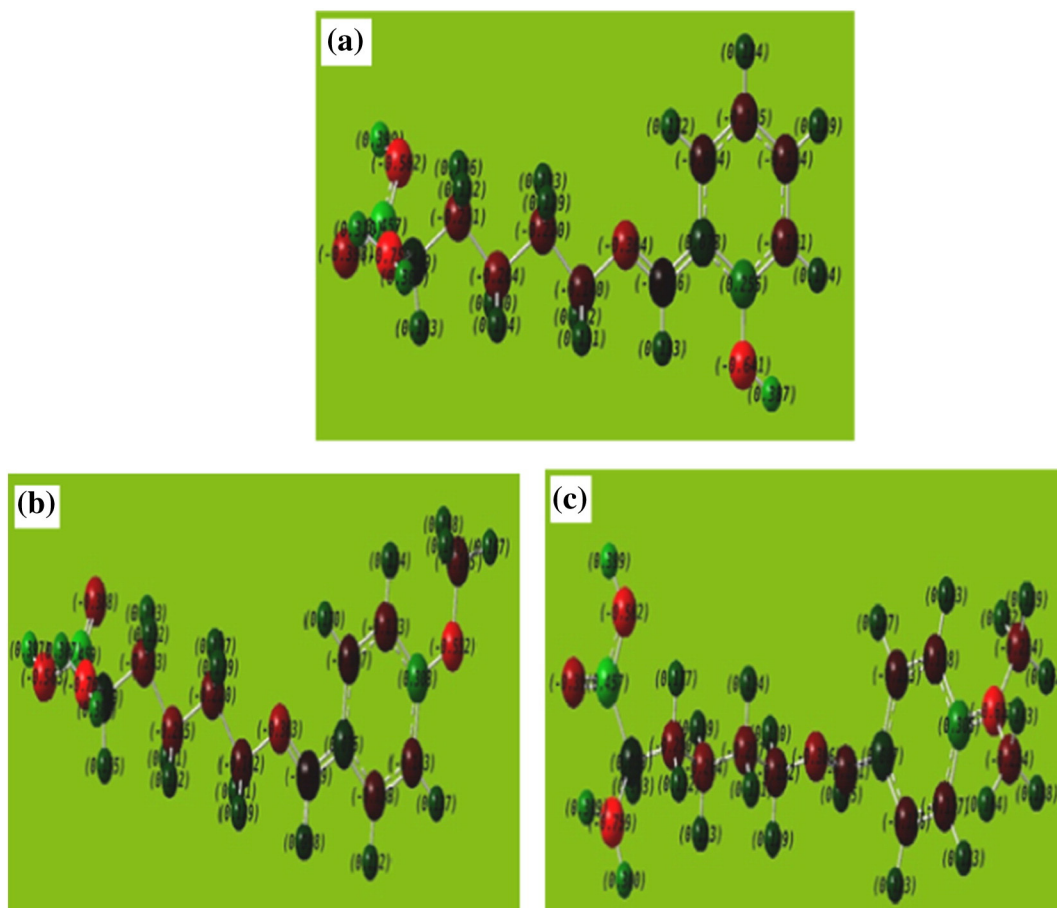


Fig. 10. a–c: Optimized structure of SBs (a) SB-1, (b) SB-2, (c) SB-3.

than that in their absence suggesting that surface smoothness increases in presence of SBs due to the formation of protective film [45].

Fig. 6(c) illustrates the bode magnitude and phase angle plots recorded for mild steel in 1 M HCl solution in absence and presence of SBs at optimum concentration. It can be seen from the Bode plots that interfacial impedance increases in presence of SBs. Moreover, bode plots that give a single narrow peak in the phase angle plot suggest a single time constant for the corrosion process at the metal–solution interface in absence and presence of SBs. It can be observed that height of the phase angle peaks increased in presence of SBs suggesting the more capacitive response of the metal/electrolyte interface due to the presence of SBs molecules at the interface [46].

3.3. Surface study

3.3.1. SEM analysis

The SEM micrographs for mild steel in absence and presence of SBs are shown in Fig. 7a–d. Fig. 7(a), represents the SEM micrograph in absence of the SBs which is severely corroded due to attack of acid on mild steel. However, in presence of SBs (Fig. 7b–d) the surface morphologies remarkably improved due to the adsorption of SBs on mild steel surface that protects the surface from acid corrosion.

3.3.2. EDX analysis

The EDX spectra of mild steel in absence and presence of SBs is shown in Fig. 8 and the results are given in Table 8. The EDX spectrum of mild steel without SBs is characterized by signals only for C and Fe. Fig. 8b–d showed the EDX spectra of mild steel in presence of different studied SBs. The EDX spectra in presence of SBs gives characteristic

additional signals for N and O which suggests that in acid solution SBs cover the mild steel that acts as barrier between metal and acid solution.

3.3.3. Atomic force microscopy

The 3D AFM micrographs of mild steel surface in absence and presence of optimum concentration of SBs are shown in Fig. 8. The AFM micrograph of mild steel surface in absence of SBs is highly damaged and severely corroded (Fig. 9(a)). However, in presence of SBs (Fig. 9b–d) the surface morphologies significantly improved due to formation of protective film by SBs. The calculated average surface roughness was 392 nm in absence of SBs, whereas in presence of SB-1, SB-2 and SB-3 the surface roughness were 167 nm, 143 nm and 84 nm, respectively. This finding again suggests that SBs form protective barrier on the mild steel surface that protects metal from the corrosion.

3.4. Quantum chemical calculation

The quantum chemical calculation was also performed to established relation between molecular structure and inhibition efficiency of investigated SBs. In last few decades' quantum chemical calculation based on the DFT theory have been proposed as a way for calculating a number of molecular parameters which are directly related to inhibition efficiency of any chemical inhibitor. Fig. 10 represents the optimized molecular structure and Fig. 11 represents the frontier molecular orbital of the investigated SBs. Some common quantum chemical indices such as, the energy of highest occupied molecular orbital (E_{HOMO}), the energy of lowest unoccupied molecular orbital (E_{LUMO}), the energy band gap (ΔE), and the dipole moment (μ) were calculated from fully optimized SBs molecules and given in Table 9. According to the Koopmans theorem the values of E_{HOMO} and E_{LUMO} related to the

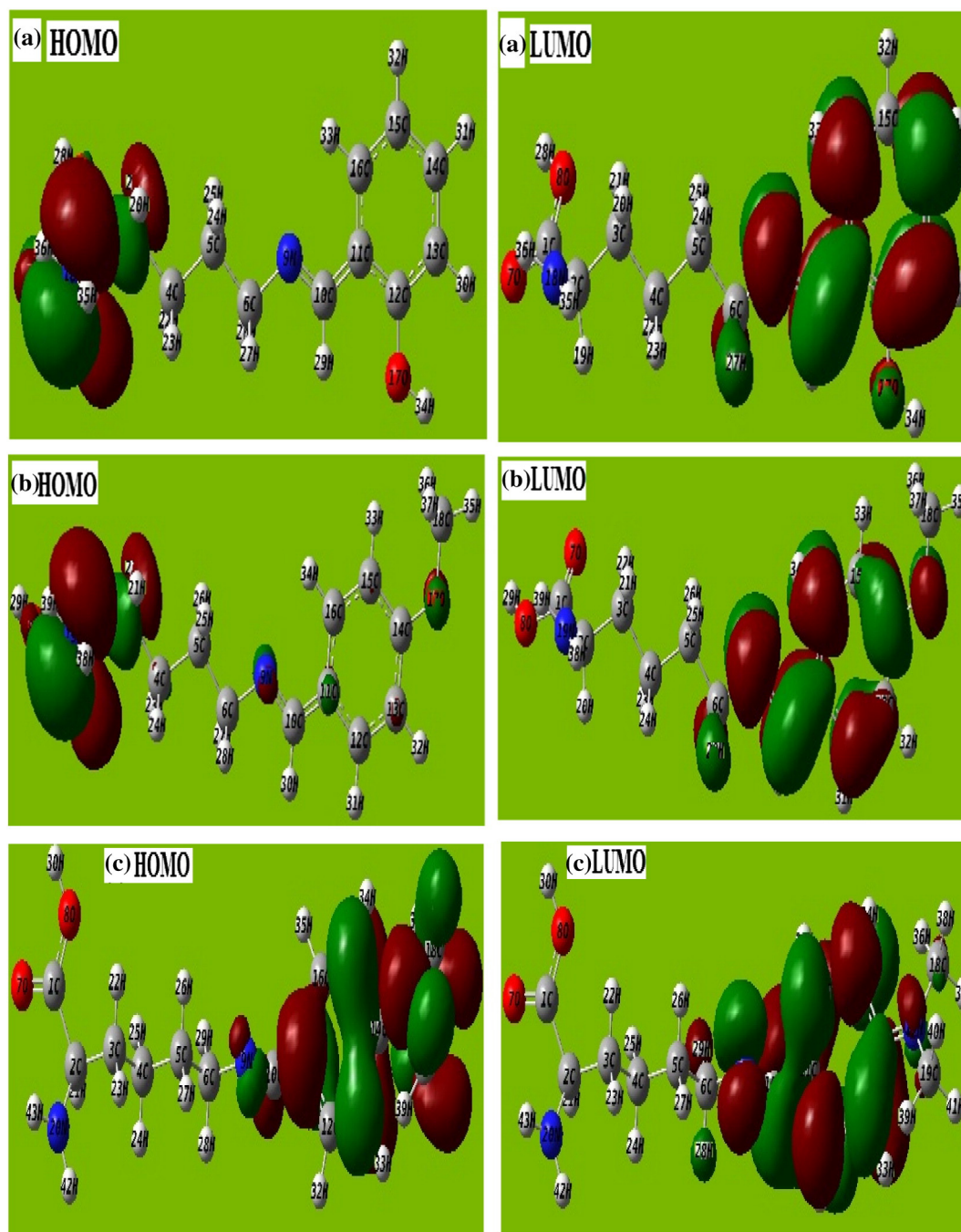


Fig. 11. a–c: The frontier molecular orbital of studied NTDs (a) SB-1 (left, HOMO; right, LUMO), (b) SB-2 (left, HOMO; right, LUMO) and (c) SB-3 (left, HOMO; right, LUMO).

ionization potential (I) and electron affinity (A) respectively as per following relations [47]:

$$I = -E_{\text{HOMO}}. \quad (9)$$

Table 9
Quantum chemical parameters of the investigated SBs.

Inhibitor	μ (Debye)	E_{HOMO} (Hartree)	E_{LUMO} (Hartree)	ΔE (Hartree)	σ	ρ
SB-1	1.1593	-0.17531	-0.00404	0.17127	0.0856	11.682
SB-2	3.4071	-0.20467	-0.03477	0.1699	0.08495	11.771
SB-3	3.8529	-0.20232	-0.04034	0.16198	0.08099	12.347

$$A = -E_{\text{LUMO}}. \quad (10)$$

The value of E_{HOMO} related to the electron donating capability of the molecules. Generally, high value of E_{HOMO} point out the nature of the molecule to provide electrons to an appropriate acceptor with vacant molecular orbitals [48,49]. In our present study the values of E_{HOMO} follow the order: SB-3 > SB-2 > SB-1 which is consisted with the order of inhibition efficiency. On the other hand a low value of E_{LUMO} associated with electron accepting tendency of the molecule from the metal surface [49,50]. Literature survey reveals that a lower value of ΔE consisted with high inhibition efficiency. In our present study the values of ΔE follow the order: SB-3 < SB-2 < SB-1 which just converse with the order of inhibition efficiency [50]. The calculated values of dipole moment (μ) are 1.1593, 3.4071 and 3.8529 Debye for SB-1, SB-2 and SB-3,

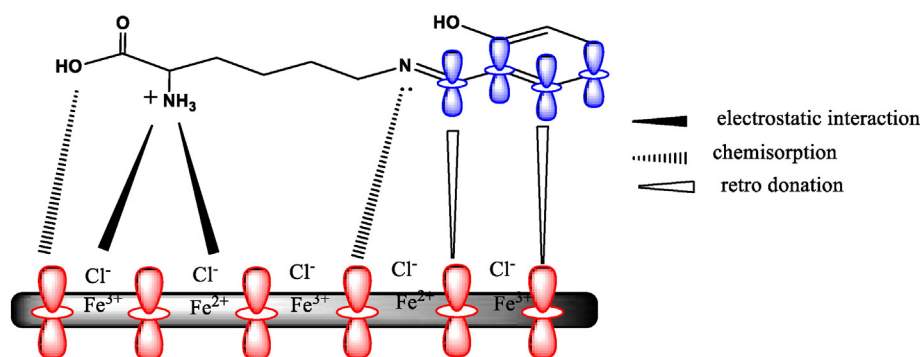


Fig. 12. Pictorial presentation of force acting between SBs and mild steel surface.

respectively. The higher dipole moment values of SBs as compared to water (1.88 Debye) suggested that SBs strongly interact with metal and form protective surface film by replacing the water present on the surface [51,52]. The values of global hardness (ρ) and global softness (σ) were calculated using the values of E_{HOMO} and E_{LUMO} as given follow [53]:

$$\rho = \frac{1}{2(I-A)} = \frac{E_{\text{LUMO}} - E_{\text{HOMO}}}{2} = \frac{\Delta E}{2}. \quad (11)$$

$$\sigma = 1/\rho. \quad (12)$$

The calculated values of global hardness and softness are given in Table 9. It is reported that magnitude of electron transfer from inhibitor to metal and therefore inhibition efficiency increases with decreasing the hardness of the inhibitor. Whereas, the high value of global softness consisted with high inhibition efficiency [54]. In our present study the values of global softness follow the order: SB-3 > SB-2 > SB-1 which is in accordance with the inhibition efficiency.

3.5. Mechanism of inhibition

It has been reported that organic compounds inhibit metal corrosion in acid solution via adsorption mechanism. The adsorption of inhibitor on the mild steel surface is influenced by several factors including chemical structure of inhibitor and charge at metal/solution interface [55,56]. The SBs can exist in protonated form in 1 M HCl solution. Moreover, due to the presence of hydrated chloride ions the surface of mild steel bears excessive negative charge, attracting the positively charged SBs [57]. The adsorption of SBs on mild steel surface takes place by two ways: first, by electrostatic attraction between positively charged SBs and negatively charged mild steel surface. The second way is the donor–acceptor interaction between neutral SBs and d-orbital of the surface Fe-atoms [58]. During first stage of adsorption, the protonated form of SBs competes with aqueous H^+ . However, after release of H_2 gas, the SBs return in their neutral form [59]. As the hetero-atoms return to their neutral form, the transfer of unshared electrons pair into d-orbital takes place [60]. However, this electron transfer causes accumulation of extra negative charge on the metal surface which renders it to transfer its electrons to the anti-bonding molecular orbitals of the SBs (retro-donation). Both donation and retro-donation strengthen adsorption of the SBs molecules on mild steel surface through synergism [61]. The pictorial presentation of the interaction responsible for adsorption of SBs on mild steel surface is shown in Fig. 12. From the weight loss, electrochemical and surface study the observed efficiency order was: SB-3 > SB-2 > SB-1. The highest inhibition efficiency of SB-3 among three studied SBs is due to presence of strong electron releasing – N (CH_3)₂ group.

4. Conclusion

The SBs were found to act as effective and green corrosion inhibitors for mild steel in 1 M HCl solution and their inhibition efficiency related with concentration and chemical structure. Among the studied SBs, the SB-3 shows the best inhibition efficiency of 95.6% at 400 mg L⁻¹ concentration.

The adsorption of SBs on mild steel surface obeys the Langmuir adsorption isotherm. The negative sign of ΔG_{ads}^0 suggests that the SBs adsorbed spontaneously on the surface. The potentiodynamic study reveals that in presence of SBs the cathodic reaction appears to be much affected than the anodic reaction suggesting that SBs act as predominantly cathodic inhibitors. SEM/EDX and AFM analyses validate the weight loss and electrochemical results. The weight loss, electrochemical and surface measurements were in good agreement.

Acknowledgment

Neeraj Kumar Gupta and Chandrabhan Verma, gratefully acknowledged Ministry of Human Resource Development (MHRD), New Delhi (India) for support.

References

- [1] Y. Sasikumar, A.S. Adekunle, L.O. Olasunkanmi, I. Bahadur, R. Baskar, M.M. Kabanda, I.B. Obot, E.E. Ebenso, *J. Mol. Liq.* 211 (2015) 105–118.
- [2] C. Verma, M.A. Quraishi, L.O. Olasunkanmi, E.E. Ebenso, *RSC Adv.* 5 (2016) 85417–85430.
- [3] M. Yadav, S. Kumar, N. Tiwari, I. Bahadur, E.E. Ebenso, *J. Mol. Liq.* 212 (2015) 151–167.
- [4] M. Yadav, S. Kumar, R.R. Sinha, I. Bahadur, E.E. Ebenso, *J. Mol. Liq.* 211 (2015) 135–145.
- [5] C. Verma, A. Singh, M.A. Quraishi, *J. Mol. Liq.* 212 (2015) 804–812.
- [6] M. Yadav, S. Kumar, I. Bahadur, D. Ramjugernath, *Int. J. Electrochem. Sci.* 9 (2014) 6529–6550.
- [7] C. Verma, E.E. Ebenso, I. Bahadur, I.B. Obot, M.A. Quraishi, *J. Mol. Liq.* 212 (2015) 209–218.
- [8] H. Vashisht, I. Bahadur, S. Kumar, K. Bharrar, D. Ramjugernath, G. Singh, *Int. J. Electrochem. Sci.* 9 (2014) 2896–2911.
- [9] C. Verma, P. Singh, M.A. Quraishi, *J. Assoc. Arab. Univ. Basic Appl. Sci.* xx (2015) <http://dx.doi.org/10.1016/j.jaubas.2015.04.003>.
- [10] H.L. Wang, H.B. Fan, J.S. Zheng, *Mater. Chem. Phys.* 77 (2002) 655–661.
- [11] M. Yadav, D. Behera, S. Kumar, R.R. Sinha, *Ind. Eng. Chem. Res.* 52 (2013) 6318–6328.
- [12] E. Naderi, M. Ehteshamzadeh, A.H. Jafari, M.G. Hosseini, *Mater. Chem. Phys.* 120 (2010) 134–141.
- [13] K.S. Jacob, G. Parameswaran, *Corros. Sci.* 52 (2010) 224–228.
- [14] M. Behpour, S.M. Ghoreishi, N. Mohammadi, N. Soltani, M.S. Niasari, *Corros. Sci.* 52 (2010) 4046–4057.
- [15] M.A. Hegazy, A.M. Hasan, M.M. Emar, M.F. Bakr, A.H. Youssef, *Corros. Sci.* 65 (2012) 67–76.
- [16] A. Asan, S. Soyulu, T. Kiyak, F. Yildırım, S.G. Oztas, N. Ancin, M. Kabasakaloglu, *Corros. Sci.* 48 (2006) 3933–3944.
- [17] S. Safak, B. Duran, A. Yurt, G. Türkoglu, *Corros. Sci.* 54 (2012) 251–259.
- [18] A.A. Farag, M.A. Hegazy, *Corros. Sci.* 74 (2013) 168–177.
- [19] L. Khandelwal, C.B. Verma, M.A. Quraishi, *J. Mater. Environ. Sci.* 6 (2015) 810–817.
- [20] K.R. Ansari, M.A. Quraishi, A. Singh, *Corros. Sci.* 79 (2014) 5–15.

- [21] A. Yurt, Ö. Aykin, *Corros. Sci.* 53 (2011) 3725–3732.
- [22] G. Gece, S. Bilgiç, *Corros. Sci.* 52 (2010) 3435–3443.
- [23] K.F. Khaled, *Corros. Sci.* 52 (2010) 3225–3234.
- [24] N.O. Eddy, *J. Adv. Res.* 2 (2011) 35–47.
- [25] K. Barouni, L. Bazzi, R. Salghi, M. Mihit, B. Hammouti, A. Albourine, S.E. Issami, *Mater. Lett.* 62 (2008) 3325–3327.
- [26] S. Issaadi, T. Douadi, A. Zouaoui, S. Chafaa, M.A. Khan, G. Bouet, *Corros. Sci.* 53 (2011) 1484–1488.
- [27] K.C. Emregül, O. Atakol, *Mater. Chem. Phys.* 82 (2003) 188–193.
- [28] M.A. Hegazy, *Corros. Sci.* 51 (2009) 2610–2618.
- [29] A.S.P. Azzouz, R.T. Ali, *Natl. J. Chem.* 37 (2010) 158–168.
- [30] C.B. Verma, M.A. Quraishi, E.E. Ebenso, *Int. J. Electrochem. Sci.* 8 (2013) 12894–12906.
- [31] D. Daoud, T. Douadi, H. Hamani, S. Chafaa, M.A. Noaimi, *Corros. Sci.* 94 (2015) 21–37.
- [32] M. Behpour, S.M. Ghoreishi, N. Soltani, M.S. Niasari, *Corros. Sci.* 51 (2009) 1073–1082.
- [33] N.I. Kairi, J. Kassim, *Int. J. Electrochem. Sci.* 8 (2013) 7138–7155.
- [34] M. Faustini, A. Maciuk, P. Salvin, C. Roos, M. Lebrini, *Corros. Sci.* 92 (2015) 287–300.
- [35] R.S.A. Hameed, E.A. Ismail, A.H. Abu-Nawwas, H.I.A. Shafey, *Int. J. Electrochem. Sci.* 10 (2015) 2098–2109.
- [36] Y.A. Albrimi, A.A. Addi, J. Douch, R.M. Souto, M. Hamdani, *Corros. Sci.* 90 (2015) 522–528.
- [37] M. Hany, A.E. Lateef, *Corros. Sci.* 92 (2015) 104–117.
- [38] C.M. Goulart, A.E. Souza, C.A.M. Huitle, C.J.F. Rodrigues, M.A.M. Maciel, A. Echevarria, *Corros. Sci.* 67 (2013) 281–291.
- [39] C. Verma, M.A. Quraishi, A. Singh, *J. Taiwan Inst. Chem. Eng.* 49 (2015) 229–239.
- [40] Q.B. Zhang, Y.X. Hua, *Electrochim. Acta* 54 (2009) 1881–1887.
- [41] A.H.A. Hamzi, H. Zarrok, A. Zarrouk, R. Salghi, B. Hammouti, S.S.A. Deyab, Guenoun, *Int. J. Electrochem. Sci.* 8 (2013) 2586–2605.
- [42] B. Zhang, C. He, C. Wang, P. Sun, F. Li, Y. Lin, *Corros. Sci.* 94 (2015) 6–20.
- [43] K.F. Khaled, N. Hackerman, *Mater. Chem. Phys.* 82 (2003) 949–960.
- [44] A.K. Singh, M.A. Quraishi, *Corros. Sci.* 53 (2011) 1288–1297.
- [45] K.M. Emran, *Int. J. Electrochem. Sci.* 9 (2014) 4217–4229.
- [46] D.K. Yadav, M.A. Quraishi, *Ind. Eng. Chem. Res.* 51 (2012) 8194–8210.
- [47] C. Verma, A. Singh, G. Pallikonda, M. Chakravarty, M.A. Quraishi, I. Bahadur, E.E. Ebenso, *J. Mol. Liq.* 209 (2015) 306–319.
- [48] P.M.A. Ivarez, J.F. García-Araya, F.J. Beltran, F.J. Masa, F. Medina, *J. Colloid Interface Sci.* 283 (2005) 503–512.
- [49] C. Verma, P. Singha, I. Bahadur, E.E. Ebenso, M.A. Quraishi, *J. Mol. Liq.* 209 (2015) 767–778.
- [50] Y. Yana, W. Li, L. Caia, B. Hou, *Electrochim. Acta* 53 (2008) 5953–5960.
- [51] M.S. Masoud, M.K. Awad, M.A. Shaker, M.M.T. El-Tahawy, *Corros. Sci.* 52 (2010) 2387–2396.
- [52] C. Verma, M.A. Quraishi, A. Singh, *J. Taiwan Inst. Chem. Eng.* 000 (2015) 1–4, <http://dx.doi.org/10.1016/j.jtice.2015.06.020>.
- [53] Z. El Adnani, M. Mcharfi, M. Sfaira, M. Benzakour, A.T. Benjelloun, M. Ebn Touhami, *Corros. Sci.* 68 (2013) 223–230.
- [54] S. Deng, X. Li, H. Fu, *Corros. Sci.* 53 (2011) 760–768.
- [55] X. Li, S. Deng, X. Xie, *J. Taiwan Inst. Chem. Eng.* 45 (2014) 1865–1875.
- [56] V. Maria, F. Bimbi, P.E. Alvarez, H. Vaca, C.A. Gervasi, *Corros. Sci.* 92 (2015) 192–199.
- [57] C. Verma, M.A. Quraishi, A. Singh, *J. Taibah Univ. Sci.* xx (2015) <http://dx.doi.org/10.1016/j.jtusc.2015.10.005>.
- [58] B. Xu, Y. Liu, X.S. Yin, W.Z. Yang, Y.Z. Chen, *Corros. Sci.* 74 (2013) 206–213.
- [59] D.K. Yadav, B. Maiti, M.A. Quraishi, *Corros. Sci.* 52 (2010) 3586–3598.
- [60] A.K. Singh, *Ind. Eng. Chem. Res.* 51 (2012) 3215–3223.
- [61] P. Singh, M.A. Quraishi, E.E. Ebenso, C.B. Verma, *Int. J. Electrochem. Sci.* 9 (2014) 7446–7459.